



LAWRENCE  
LIVERMORE  
NATIONAL  
LABORATORY

# Benchmark Measurements of the Ionization Balance of Non-LTE Gold

R. F. Heeter, S. B. Hansen, K. B. Fournier, M. E. Foord,  
D. H. Froula, A. J. Mackinnon, M. J. May, M. B.  
Schneider, B. K. F. Young

May 22, 2007

Physical Review Letters

## **Disclaimer**

---

This document was prepared as an account of work sponsored by an agency of the United States government. Neither the United States government nor Lawrence Livermore National Security, LLC, nor any of their employees makes any warranty, expressed or implied, or assumes any legal liability or responsibility for the accuracy, completeness, or usefulness of any information, apparatus, product, or process disclosed, or represents that its use would not infringe privately owned rights. Reference herein to any specific commercial product, process, or service by trade name, trademark, manufacturer, or otherwise does not necessarily constitute or imply its endorsement, recommendation, or favoring by the United States government or Lawrence Livermore National Security, LLC. The views and opinions of authors expressed herein do not necessarily state or reflect those of the United States government or Lawrence Livermore National Security, LLC, and shall not be used for advertising or product endorsement purposes.

# Benchmark measurements of the ionization balance of non-LTE gold

R.F. Heeter, S.B. Hansen, K.B. Fournier, M.E. Foord, D.H.  
Froula, A.J. Mackinnon, M.J. May, M.B. Schneider, B.K.F. Young  
*Lawrence Livermore National Laboratory,*  
*P.O. Box 808, L-473, Livermore, CA 94550, USA*

(Dated: May 22, 2007)

## Abstract

We present a series of benchmark measurements of the ionization balance of well characterized gold plasmas with and without external radiation fields at electron densities near  $10^{21}$  cm $^{-3}$  and various electron temperatures spanning the range 0.8 to 2.4 keV. We have analyzed time- and space-resolved M-shell gold emission spectra using a sophisticated collisional-radiative model with hybrid level structure, finding average ion charges  $\langle Z \rangle$  ranging from 42 to 50. At the lower temperatures, the spectra exhibit significant sensitivity to external radiation fields and include emission features from complex N-shell ions not previously studied at these densities. The measured spectra and inferred  $\langle Z \rangle$  provide a stringent test for non-local thermodynamic equilibrium (non-LTE) models of complex high- $Z$  ions.

Understanding the atomic physics and plasma processes involved in the x-ray emission and absorption of complex ions is a critical component of predictive modeling for high- $Z$ , high-energy-density (HED) plasmas. For applications such as laser-driven inertial confinement fusion (ICF), which has come to rely on high- $Z$  hohlraums to efficiently symmetrize and transfer energy from the laser driver to a target capsule [1], there is particular interest in the atomic and radiation physics near the critical density for optical laser light. At such densities, the simplifying assumption of local thermodynamic equilibrium (LTE) is not valid and reliable non-LTE calculations are required. These calculations are, however, notoriously difficult, as dramatically illustrated at the first non-LTE code comparison workshop [2], where contributed predictions for the average ionization of gold spanned more than 20 charge states. Benchmark laser-plasma measurements at NOVA found average gold charge states  $\langle Z \rangle$  near 50 for electron temperatures  $T_e$  of 2 – 2.6 keV and densities  $n_e$  near  $10^{20}$  cm $^{-3}$  [3, 4]. Coronal-limit measurements at the Livermore electron beam ion trap (EBIT) found  $\langle Z \rangle$  near 47 at  $T_e=2.5$  keV and  $n_e = 10^{12}$  cm $^{-3}$  [5]. These measurements stimulated significant efforts to advance non-LTE modeling capabilities: the agreement among codes at subsequent workshops improved to within  $\approx 10$  charge states [6, 7] due largely to increasing emphasis on dielectronic recombination [5] and model completeness [8, 9]. The most recent non-LTE code comparison workshop [10] saw good agreement among codes near closed shell ions for a variety of test cases, but disagreement up to 10 charge states for open-shell high- $Z$  ions persists. Since the existing laser-plasma benchmark values for Au  $\langle Z \rangle$  lie near the stable Ni-like ion Au $^{51+}$  in a temperature regime where achievable external radiation fields ( $T_r \approx 200$ eV) have little influence on  $\langle Z \rangle$ , they provide neither a stringent test of non-LTE codes in the most difficult regime nor clear information on the response of high- $Z$  plasmas to external radiation. And although the low-density EBIT measurement lies well into the  $N$  shell, it does not access the multiply excited configurations that play an important role in collisional-radiative kinetics at the densities most relevant to predictive modeling of energy transfer and radiation flow in ICF plasmas. The present work extends the benchmark NOVA data to lower electron temperatures, moving the gold plasma into a regime where it is sensitive to a moderate  $T_r$  and  $\langle Z \rangle$  solidly into the  $N$  shell.

The experiments were performed at the OMEGA laser (Laboratory for Laser Energetics, University of Rochester), where beams of 351 nm light at intensities  $I = 1 - 7 \times 10^{14}$  W/cm $^2$  irradiated the surface of target disks composed of 200  $\mu$ m-diameter, 0.5  $\mu$ m thick layers of

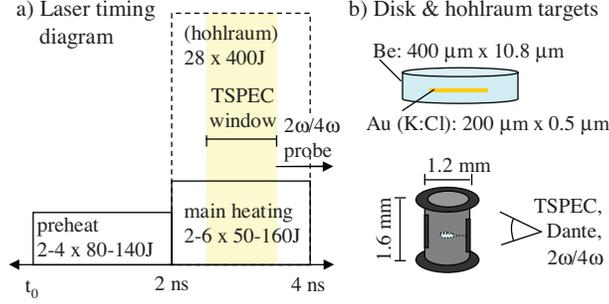


FIG. 1: a) Diagram showing the timing and number of beams used for direct disk preheat, main disk heating, and hohlraum heating along with the timing of the TSPEC and Thomson scattering measurements. b) Target diagrams and dimensions and the orientation of diagnostics.

Au or Au+K:Cl comix surrounded by 400  $\mu\text{m}$ -diameter, 10.8  $\mu\text{m}$  thick Be disks. The laser deposited 0.26 - 1.5 kJ over 4 ns in a fixed laser spot size of 280  $\mu\text{m}$  (geometric), directly heating the targets to the desired temperatures. Some of the targets were also indirectly heated by placement inside 1.6  $\times$  1.2 mm tungsten-coated hohlraums. Figure 1 gives the laser schematics of the targets and the timing of direct and hohlraum laser heating.

The plasma conditions were diagnosed using a complete set of independent measurements: Thomson scattering (TS) diagnostics with 50 J probe beams at  $2\omega$  and  $4\omega$  [11] were fielded on a subset of the experiments, giving measured  $T_e$  that follow roughly the intensity scaling predicted by Lindl [1] as shown in Fig. 2. The best-fit line to the TS data,  $T_e(\text{keV}) = 0.67 \times [I/10^{14} \text{ W/cm}^2]^{2/3}$ , was used to determine  $T_e$  for all of the experimental measurements. Another electron temperature measurement was provided by K-shell K and Cl spectra, which were recorded along with the M-shell Au spectra by a time-gated, spatially resolved, and relatively calibrated spectrometer with resolution of  $E/\Delta E \approx 240$ . In conjunction with pinhole imaging showing minimal target expansion in the radial direction [12], the axial expansion was used to determine the ion density to within 20% at the time of the spectroscopic measurements ( $t_m$ ). Assuming charge neutrality, the electron density was found using the measured average ion charge for Au (and K:Cl when present). Finally, the radiation field was measured to be 185 eV over 61% of the solid angle seen by the sample using Dante [13], an absolutely calibrated multi-channel filtered diode array. More detail on the experimental setup and instrumentation is given in Refs. [12, 14].

K-shell emission spectra from the Au+K:Cl co-mix targets were analyzed with collisional-

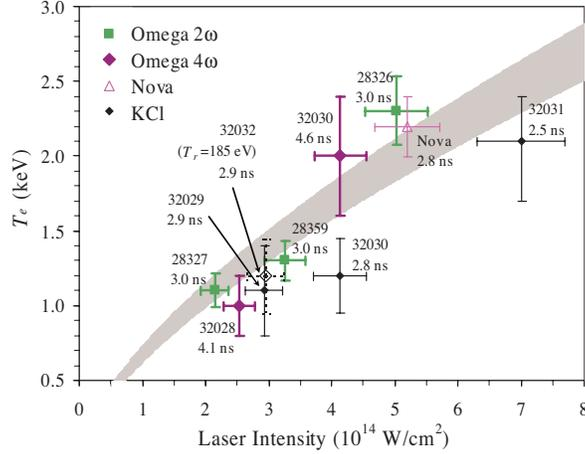


FIG. 2: (color online) Electron temperature measurements from Thomson scattering and spectroscopy of K:Cl tracers at various laser intensities, along with shot numbers and measurement times. The gray region is the best fit of the TS data to an  $I^{2/3}$  intensity scaling with width corresponding to 10% experimental uncertainty in  $I$ . The measured  $T_e$  of the  $5.2 \times 10^{14} \text{ W/cm}^2$  case is in good agreement with the previous Nova experiment [3].

radiative models [15] based on data from the Flexible Atomic Code (FAC) [16]. The K-shell K and Cl models include singly excited states up to  $n = 6$  and doubly excited states up to  $n = 4$  for H- through Be-like ions, with self-consistent opacity effects modeled using the the escape factor formalism for a  $200 \mu\text{m}$  slab and the external radiation field in the hohlraum-enclosed measurements modeled by a 185 eV blackbody with a dilution factor of 0.61. Since equilibration between He- and H-like K and Cl ions can take several ns at the measured electron densities, time-dependent effects are approximated by setting H-like ion populations to zero at the onset of the main heating beams ( $t = 2 \text{ ns}$ ) and solving for time-dependent ion populations using rates determined by the measured  $n_e$  and  $T_r$  at  $t_m$  at various constant  $T_e$ . The K:Cl temperature is diagnosed by finding the best fit to the time-gated experimental data of time-dependent synthetic spectra integrated over  $t_m \pm 100 \text{ ps}$ . These temperatures are plotted along with the TS measurements in Fig. 2 with error bars determined by the spread of the best-fit temperatures to three diagnostic line ratios. The spectroscopic temperatures from  $t_m = 2.5 - 2.9 \text{ ns}$  tend to fall below the temperatures measured by Thomson scattering ( $3.0 - 4.6 \text{ ns}$ ), suggesting that  $T_e$  may be increasing at the time of the spectroscopic measurements. Temperatures diagnosed using steady-state K-shell

diagnostics would be  $\approx 10\%$  lower still.

To better understand the time-dependence of the sample expansion and temperature, we have performed a 2-dimensional radiation-hydrodynamic simulation with the LASNEX code [17] for one of the Au:KCl co-mix samples (shot 32030). The laser power was delivered to both faces of the target by cone 1 OMEGA beams incident to the target faces at an angle of  $21.4^\circ$  with respect to the sample axis and absorbed via inverse bremsstrahlung; each face of the target sees two preheat beams with 135 J/beam and three main heating beams with 68 J/beam. The simulation gives densities consistent with the experimental measurements temperatures of 1.15 keV at the end of the 2 ns preheat pulse and 1.25 keV at the time of the spectroscopic measurement  $t_m = 2.8$  ns; supporting the notion that  $T_e$  is rising between the time of the spectroscopic measurements and the time of the Thomson scattering measurements (particularly those at  $4\omega$ ). However, the variation in the simulated  $T_e$  is gentle enough, and the equilibration between the dominant Au ions is rapid enough ( $< 0.1$  ns), that we may consider the Au ions to be in the steady state during the 0.2 ns duration of the spectroscopic measurements.

To determine the average ion charge  $\langle Z \rangle$  of the measured Au spectra, we have constructed a hybrid fine-structure/UTA model [18] of Fe- to Sr-like Au based on data from the FAC code [16]. For  $(n)^N$  denoting a superconfiguration with occupation number  $N$  and principle quantum number  $n$ , the modeled level structure for Fe- to Ni-like Au ions includes all possible configurations in  $(1)^2(2)^8(3)^N$  and  $(1)^2(2)^8(3)^{N-1}(n)^1$  with  $n = 4 - 7$ . The Ni-like ion includes additionally all possible double excitations in the superconfiguration  $(1)^2(2)^8(3)^{16}(4)^1(n)^1$  with  $n = 4 - 5$  to account for prominent  $3d^84l5f - 3d^94l$  emission features to the blue of the dominant  $3d^95f - 3d^{10}$  lines [3, 20]. The Zn- through Ge-like ions include all possible configurations in  $(1)^2(2)^8(3)^{18}(4)^N$ ,  $(1)^2(2)^8(3)^{18}(4)^{N-1}(n)^1$  with  $n = 4 - 7$ , and  $(1)^2(2)^8(3)^{17}(4)^N(n)^1$  with  $n = 4 - 6$ . Ga- through Sr-like ions are modeled with similar structure but exclude configurations with more than one  $4f$  electron. For all ions, a ‘coronal’ subset of the relativistic configurations, defined as those configurations accessible through single-electron excitation from the ground configuration, is replaced by detailed fine structure levels to form the hybrid model. Transitions among these fine structure levels include configuration interaction effects and thus have more accurate energies and strengths than the unresolved transition arrays (UTAs) they replace in the hybrid model; this accuracy is extended to the remaining UTAs in each ion by applying energy shifts and

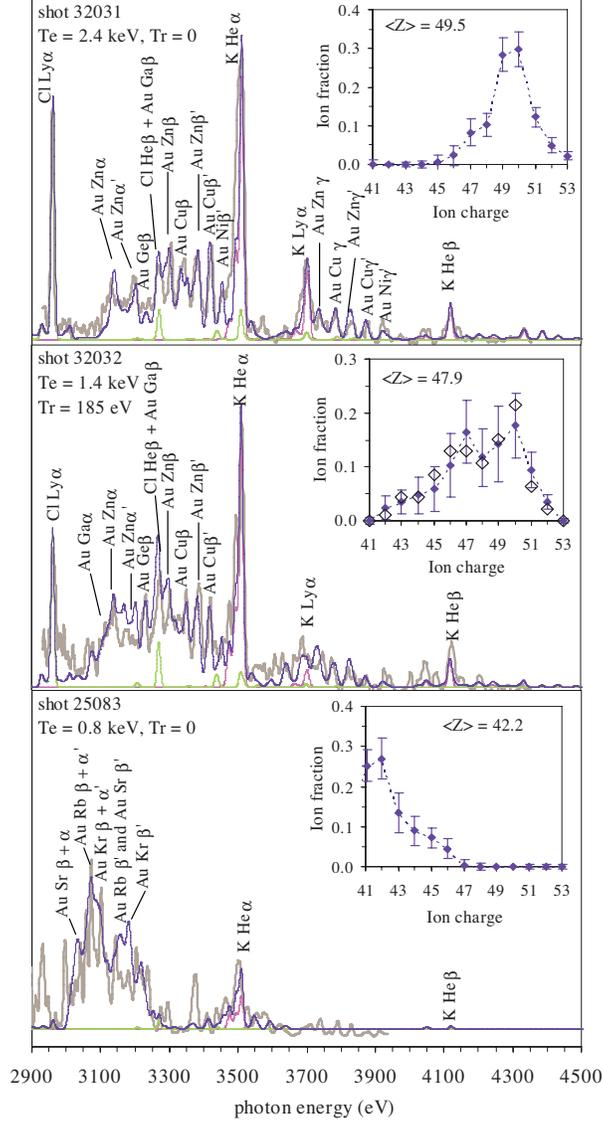


FIG. 3: (color online) Experimental data (thick gray lines) overlaid with modeled emission (thin blue lines) which includes the diagnostic K-shell K and Cl spectra (magenta and green lines, respectively) and the best-fit M-shell Au emission obtained using the inset charge state distribution. The CSD from shot 25086 is given by hollow diamonds in the inset of the central plot. The dominant components of selected M-shell emission features are labeled by parent ion, isoelectronic sequence, and transition type:  $\alpha = 4p_{3/2} - 3s_{1/2}$ ,  $\alpha' = 4d_{3/2} - 3p_{1/2}$ ,  $\beta = 5f_{7/2} - 3d_{5/2}$ ,  $\beta' = 5f_{5/2} - 3d_{3/2}$ ,  $\gamma = 6f_{7/2} - 3d_{5/2}$ , and  $\gamma' = 6f_{5/2} - 3d_{3/2}$ . The feature at 3375 eV in shot 25083 may be an experimental artifact.

TABLE I: Laser intensities and plasma conditions at the time of the M-band Au measurements ( $t_m$ ), inferred average Au ion charge, and width  $\sigma_Z$  of the CSD. The tabulated  $T_e$  have error bars of +15% and -25% due to uncertainties in the laser intensities, the use of a scaled fit to Thomson scattering data for  $T_e$ , and the possibility that  $T_e$  was below its intensity-scaled value at  $t_m$ .

shot	$I(10^{14}$ W/cm <sup>2</sup> )	$T_e$ (keV)	$T_r$ (eV)	$n_e(10^{20}$ cm <sup>-3</sup> )	$t_m$ (ns)	Au $\langle Z \rangle$	$\sigma_Z$
25083	1.4	0.8	0	7	2.7	$42.2 \pm 1.2$	2.6
25082	1.4	0.8	185	11	2.6	$45.3 \pm 1.5$	2.3
32029	2.9	1.4	0	10	2.9	$46.8 \pm 1.2$	5.0
25086	2.9	1.4	185	9	2.7	$47.8 \pm 1.4$	5.4
32032	2.9	1.4	185	10	2.9	$47.9 \pm 1.4$	5.8
32030	4.1	1.7	0	7	2.8	$48.8 \pm 0.7$	2.6
Ref.[3]	5.2	2.0	0	6	2.8	$49.3 \pm 0.5$	1.5
25080	5.2	2.0	185	6	2.6	$49.6 \pm 0.5$	1.1
32031	7.0	2.4	0	6	2.5	$49.5 \pm 0.5$	2.1
Ref.[4]	–	2.6	190	14	1.6	$50.5 \pm 1.0$	2.0

oscillator strength factors determined for the underlying  $n\ell j - n'\ell'j'$  transitions.

To determine the steady-state populations in the resultant set of  $2.1 \times 10^6$  mixed levels, we construct the full collisional-radiative rate matrix and follow the averaging procedure detailed in Ref [18] to obtain and solve a smaller rate matrix for an averaged model. We then restore the full model, finding the populations of the averaged levels from stored configuration-to-level rates in a procedure roughly based on Ref. [19]. The spectra obtained from the hybrid model are in very good agreement with spectra from a restricted, tractable fine structure model of Co- to Cu-like ions. Since a similarly complete fine structure model of Fe- to Sr-like ions would have more than  $10^{10}$  levels, the computational efficiencies of the hybrid scheme are essential.

Determining the experimental charge state distribution (CSD) by fitting the calculated emission from each ion to the experimental data is not trivial: each ion contributes 3-6 significant features to the 2.9-3.6 keV spectral range and there is significant overlap between

the emission from different ions. We have thus employed a genetic algorithm [15, 21] to search a wide range of possible CSDs seeking the best fit to 27 points in the 2.9-3.6 keV spectral range. We fit the experimental data twice: first using the emission features computed by the hybrid model with its own CSD at the measured (constant)  $n_e$ ,  $T_e$ , and  $T_r$ . This best-fit CSD is used to constrain a second calculation of the emission for each ion, thus ensuring consistency in the calculated opacity effects and the relative contributions of recombination, direct excitation, and ionization processes to the emission features. We find that, as in [3], opacity effects reduce the intensities of the 5-3 emission features by as much as  $\approx 20\%$ . The effect of enforcing the first-pass CSD on the spectral features is most significant at low temperatures where dielectronic rates into the upper levels of the 5-3 transitions ( $\Delta E \approx 1$  keV) tend to dominate over direct collisional excitation ( $\Delta E \approx 3$  keV), and is more significant than variations of 10% in temperature or density. Error bars for the fractional ion population are the sum of the standard errors from three sources: 1) fit uniqueness as determined by five different trials of the genetic algorithm, 2) a  $\pm 50\%$  uncertainty in the emission intensity per ion on either side of the Ge-/As-like ion divide associated with the exclusion of states with more than one  $4f$  electron in As- through Sr-like ions, and 3) differences in the first- and second-pass CSDs which reflect uncertainty in opacity effects and population mechanisms. Error bars on the final average  $\langle Z \rangle$  incorporate all three standard errors at fixed conditions. Since equilibration times among the dominant Au ions are shorter than 0.1 ns, there is no additional uncertainty in  $\langle Z \rangle$  due to time-dependent effects.

Figure 3 shows three experimental spectra with the best-fit modeled data along with insets giving the inferred charge state distributions. Each M-shell ion contributes two  $5f - 3d$  features separated by  $\approx 80$  eV and several  $4p - 3s$  and  $4d - 3p$  features at lower energies. With decreasing ion charge, the  $5f - 3d$  features are redshifted by  $\approx 40$  eV per ion and the separation between 5-3 and 4-3 features decreases. The complete results of the fitting to all experimental spectra are summarized in Table I. Two shots with similar plasma conditions, 25086 and 32032, indicate good reproducibility in the experimental data and fitting procedure. The low-temperature,  $T_r = 0$  case assumes that 15% of the ions have a charge of 40 or less in ions that were not modeled. The effect of the external radiation field is most significant at low  $T_e$ , where collisional excitation and ionization rates are not dramatically larger than photoexcitation and photoionization rates.

These benchmark measurements of  $\langle Z \rangle$  and M-shell emission spectra across a wide range

of  $T_e$  and  $T_r$  can be used to test and verify non-LTE models of complex, high- $Z$  ions. Improved understanding of the internal energy, radiative properties, and interaction with external radiation fields of non-LTE high- $Z$  ions could have a significant impact on ICF science. The presented analysis also demonstrates the efficacy of a hybrid model for providing spectroscopic-quality emission from N-shell ions for which UTA models would be inaccurate and fine-structure models would be intractable.

We thank the crew of the Omega laser at the University of Rochester Laboratory for Laser Energetics for expertly executing these experiments.

This work was performed under the auspices of the U.S. Department of Energy by University of California Lawrence Livermore National Laboratory under contract No. W-7405-Eng-48.

- 
- [1] J. Lindl, *Phys. Plasmas* **2**, 3933 (1995). (Scaling law given on p. p. 3995.)
  - [2] R.W. Lee, J.K. Nash, and Y. Ralchenko, *J. Quant. Spectrosc. Rad. Transf.* Vol. **58**, 131 (1997).
  - [3] M.E. Foord, S.H. Glenzer, R.S. Thoe, K.L. Wong, K.B. Fournier, B.G. Wilson, and P.T. Springer, *Phys. Rev. Lett.* **85**, 992 (2000); M.E. Foord *et al.*, *J. Quant. Spectrosc. Rad. Transf.* Vol. **65**, 231 (2000).
  - [4] S.H. Glenzer, K.B. Fournier, B.G. Wilson, R.W. Lee, and L.J. Suter, *Phys. Rev. Lett.* **85**, 045002 (2001),
  - [5] K.L. Wong, M.J. May, P. Beiersdorfer, K.B. Fournier, B. Wilson, G.V. Brown, P. Springer, P.A. Neill, and C.L. Harris *Phys. Rev. Lett.* **90**, 235001 (2003),
  - [6] C. Bowen, A. Decoster, C.J. Fontes, K.B. Fournier, O. Peyrusse, and Yu.V. Ralchenko, *J. Quant. Spectrosc. Rad. Transf.* Vol. **81**, 70 (2003).
  - [7] C. Bowen, R.W. Lee, Yu. Ralchenko, *J. Quant. Spectrosc. Rad. Transf.* Vol. **99**, 102 (2006).
  - [8] O. Peyrusse, C. Bauche-Arnoult, and J. Bauche, *J. Phys. B* **38**, L137 (2005).
  - [9] Z. Wu, J. Pang, and J. Yan, *J. Quant. Spectrosc. Rad. Transf.* Vol. **102**, 402 (2006).
  - [10] J Rubiano *et al.* (to be published).
  - [11] S. H. Glenzer *et al.* *Phys. Rev. Lett.* **77**, 1496 (1996); **79**, 1277 (1997); **82**, 97 (1999); **86**, 2565 (2001) and D. H. Froula *et al.*, *Phys. Rev. Lett.* **88**, 105003 (2002).
  - [12] R.F. Heeter *et al.*, *Proceedings of Inertial Fusion Sciences and Applications 2003*, published

- by American Nuc. Soc., p. 1018.
- [13] H.N. Kornblum, R.L. Kauffman, and J.A. Smith, *Review of Scientific Instruments*, **57**, 2179 (1986).
  - [14] R.F. Heeter *et al.*, *Proceedings of Atomic Processes in Plasmas 2004* edited by J.S. Cohen, S. Mazevet, and D.P. Kilcrease, p. 103.
  - [15] S.B. Hansen, Ph.D. thesis, University of Nevada, Reno, 2003.
  - [16] M.F. Gu, *Ap. J.* **582**, 1241 (2003).
  - [17] G. Zimmerman and W.Kruer, *Comments Plasma Phys. Control. Fusion* **2**, 51 (1975).
  - [18] S.B. Hansen, J. Bauche, C. Bauche-Arnoult, and M.F. Gu, (to be published).
  - [19] F.B. Rosmej, *Europhys. Lett.* **76**, 1081 (2006).
  - [20] C. Bauche-Arnoult *et al.*, *Phys. Rev. A* **33**, 791 (1986).
  - [21] I.E. Golovkin, R.C. Mancini, S.J. Luis, R.W. Lee, and L. Klein, *J. Quant. Spectrosc. Rad. Transf. Vol.* **75**, 625 (2002).